

# DEEP LEAST-SQUARES METHODS: AN UNSUPERVISED LEARNING-BASED NUMERICAL METHOD FOR SOLVING ELLIPTIC PDES\*

ZHIQIANG CAI<sup>†</sup>, JINGSHUANG CHEN<sup>†</sup>, MIN LIU<sup>‡</sup>, AND XINYU LIU<sup>†</sup>

**Abstract.** This paper studies an unsupervised deep learning-based numerical approach for solving partial differential equations (PDEs). The approach makes use of the deep neural network to approximate solutions of PDEs through the compositional construction and employs least-squares functionals as loss functions to determine parameters of the deep neural network. There are various least-squares functionals for a partial differential equation. This paper focuses on the so-called first-order system least-squares (FOSLS) functional studied in [3], which is based on a first-order system of scalar second-order elliptic PDEs. Numerical results for second-order elliptic PDEs in one dimension are presented.

**Key words.** Deep Least-Squares Method, Neural Network, Elliptic PDEs

**AMS subject classifications.**

**1. Introduction.** Recently, deep neural network (DNN) models have had great success in computer vision, pattern recognition, and many other artificial intelligence tasks. A special feature of DNN is its new way to approximate functions through a composition of multiple linear and activation functions. This leads to some recent studies (see, e.g., [2, 5, 6, 12]) on applications of deep learning to partial differential equations (PDEs).

The idea of solving differential equations using neural networks may be traced back to a paper in 1994 by Dissanayake and Phan-Thien [4]. For a differential equation  $L(u) = 0$  defined on the domain  $\Omega$  with boundary condition  $B(u) = 0$  on  $\partial\Omega$ , a neural network was trained to minimize the following least-square functional

$$(1.1) \quad \tilde{\mathcal{L}}(v) = \int_{\Omega} |L(v)(x)|^2 dx + \int_{\partial\Omega} |B(v)(x)|^2 dS.$$

Several follow-up work uses similar idea with one hidden layer and samples points from a mesh to numerically approximate the integrals in  $\mathcal{L}$  at each epoch [9, 10, 11]. More recently, there is a limited by emerging literature on the use of deeper hidden layers to solve PDEs [2, 5, 12]. It is also illustrated that the training points can be obtained by a random sampling of the domain rather than using a mesh, which is beneficial in higher-dimensional problem [2, 12]. The least-squares functional defined in (1.1) is based on the original PDEs. For a second order PDEs, the minimization of  $\tilde{\mathcal{L}}(v)$  over admissible functions leads to a fourth-order PDEs, which is a more difficult problem than the original one. Moreover, the interior and the boundary integrals in (1.1) are not balanced.

Another formulation of the loss function is to use the energy functional of the underlying PDEs, such as the resulting deep Ritz method recently introduced by E-Yu [6]. For a Poisson problem with Dirichlet boundary conditions, the energy functional is given by

$$(1.2) \quad \tilde{\mathcal{J}}(v) = \int_{\Omega} \left( \frac{1}{2} |\nabla v(x)|^2 - f(x)v(x) \right) dx.$$

This approach is applicable to problems having underlying minimization principle.

The purpose of this paper is to study an unsupervised deep learning-based numerical approach for solving PDEs. The approach makes use of the deep neural network to approximate solutions of

\*Submitted to the editors DATE.

<sup>†</sup>Department of Mathematics, Purdue University, 150 N. University Street, West Lafayette, IN 47907-2067 (caiz@purdue.edu, chen2042@purdue.edu, liu1957@purdue.edu).

<sup>‡</sup>Department of Mechanical Engineering, Purdue University, 585 Purdue Mall, West Lafayette, IN 47907-2088(liu66@purdue.edu)

PDEs through the compositional construction and employs least-squares (LS) functionals as loss functions to determine parameters of the deep neural network. There are various least-squares functionals for a partial differential equation, this paper focuses on the FOSLS functional studied in [3], which is based on a first-order system of scalar second-order elliptic PDEs.

The LS methodology has been intensively studied for many PDEs including problems arising from solid and fluid dynamics, radiation transport, magnetohydrodynamics, etc. The method has many attractions. The two striking features are (i) it naturally symmetrizes and stabilizes the original problem; and (ii) the corresponding LS functional is an accurate a posteriori error estimator. The first property enables us to work on complex systems which might not have underlying minimization principles, and the second one provides feedback for automatically controlling numerical processes such as the numbers of neurons and layers in the deep neural networks, the number and the location of sampling points for evaluating LS functional.

The paper is organized as follows. Section 2 describes the second order elliptic PDEs, the least-squares formulation based on a first-order system of the underlying problem introduced in [3], and proper treatment of boundary conditions when using energy, LS, and FOSLS functionals. Section 3 introduces deep neural network and corresponding deep FOSLS method. Finally, numerical results on three test problems in one dimension are presented in section 4.

**2. Problem Formulation.** Let  $\Omega$  be a bounded domain in  $\mathbb{R}^d$  with Lipschitz boundary  $\partial\Omega = \bar{\Gamma}_D \cup \bar{\Gamma}_N$ . Consider the following second-order scalar elliptic partial differential equation:

$$(2.1) \quad -\operatorname{div}(A\nabla u) + Xu = f, \quad \text{in } \Omega$$

with boundary conditions

$$(2.2) \quad u = g_D, \quad \text{on } \Gamma_D \quad \text{and} \quad -\mathbf{n} \cdot A\nabla u = g_N, \quad \text{on } \Gamma_N,$$

where  $f \in L^2(\Omega)$ ,  $g_D \in H^{1/2}(\Gamma_D)$ ,  $g_N \in H^{-1/2}(\Gamma_N)$ ;  $A(x)$  is an  $n \times n$  symmetric matrix of functions in  $L^2(\Omega)$ ;  $X$  is a linear differential operator of order at most one; and  $\mathbf{n}$  is the outward unit vector normal to the boundary. We assume that  $A$  is uniformly positive definite. Possible choices for  $X$  include:  $Xu = \operatorname{div}(\mathbf{b}u)$  with  $\mathbf{b} \in L^2(\Omega)^d$  and  $Xu = \mathbf{a} \cdot \nabla u + cu$  with  $\mathbf{a} \in L^2(\Omega)^d$ ,  $c(x) \in L^2(\Omega)$ .

Here and thereafter, we use the standard notation and definitions for the Sobolev space  $H^s(\Omega)$  and  $H^s(\Gamma)$  for a subset  $\Gamma$  in  $\partial\Omega$ . The standard associated inner product and norms are denoted by  $(\cdot, \cdot)_{s,\Omega}$  and  $(\cdot, \cdot)_{s,\Gamma}$  and by  $\|\cdot\|_{s,\Omega}$  and  $\|\cdot\|_{s,\Gamma}$ , respectively. When  $s = 0$ ,  $H^0(\Omega)$  coincides with  $L^2(\Omega)$ . Denote the corresponding norms on product space  $H^s(\Omega)^d$  by  $\|\cdot\|_{s,\Omega,d}$  and  $|\cdot|_{s,\Omega,d}$ . When there is no ambiguity, the subscript  $\Omega$  and  $d$  in the designation of norms will be suppressed.

**2.1. Least-Squares Formulations.** Problem (2.1)-(2.2) is non-symmetric in general and, hence, has no underlying minimization principle. To make use of the deep neural network, we will employ LS principles. There are many LS formulations for problem (2.1). For example, a direct application of the LS principle to problem (2.1) leads to a LS functional defined in (2.14) which is similar to that in (1.1) but with different boundary terms. In this section, we describe the FOSLS formulation introduced in [3] which is based on a first-order system of problem (2.1)-(2.2).

To this end, introducing the flux variable  $\boldsymbol{\sigma} = -A\nabla u$ , the second-order problem in (2.1) may be rewritten as a first-order system:

$$(2.3) \quad \begin{cases} \operatorname{div} \boldsymbol{\sigma} + Xu = f, & \text{in } \Omega, \\ \boldsymbol{\sigma} + A\nabla u = \mathbf{0}, & \text{in } \Omega \end{cases}$$

with boundary conditions

$$(2.4) \quad u = g_D, \quad \text{on } \Gamma_D \quad \text{and} \quad \mathbf{n} \cdot \boldsymbol{\sigma} = g_N, \quad \text{on } \Gamma_N.$$

Let

$$H(\operatorname{div}; \Omega) \equiv \{ \mathbf{v} \in L^2(\Omega)^d : \operatorname{div} \mathbf{v} \in L^2(\Omega) \}.$$

Denote subsets of  $H^1(\Omega)$  and  $H(\operatorname{div}; \Omega)$  satisfying non-homogeneous boundary conditions by

$$H_{D,g}^1(\Omega) = \{ v \in H^1(\Omega) : v|_{\Gamma_D} = g_D \} \text{ and } H_{N,g} = \{ \boldsymbol{\tau} \in H(\operatorname{div}; \Omega) : \boldsymbol{\tau} \cdot \mathbf{n}|_{\Gamma_N} = g_N \}$$

respectively. When  $g_D = 0$  and  $g_N = 0$ , these subsets become subspaces and are denoted by  $H_D^1(\Omega)$  and  $H_N(\operatorname{div}; \Omega)$ . Let

$$\mathcal{V}_g = H_{N,g}(\operatorname{div}; \Omega) \times H_{D,g}^1(\Omega) \quad \text{and} \quad \mathcal{V}_0 = H_N(\operatorname{div}; \Omega) \times H_D^1(\Omega),$$

then the FOSLS formulation is to find  $(\boldsymbol{\sigma}, u) \in \mathcal{V}_g$  such that

$$(2.5) \quad \tilde{\mathcal{G}}(\boldsymbol{\sigma}, u; \mathbf{f}) = \min_{(\boldsymbol{\tau}, v) \in \mathcal{V}_g} \tilde{\mathcal{G}}(\boldsymbol{\tau}, v; \mathbf{f}),$$

where  $\mathbf{f} = (f, g_D, g_N)$  and the FOSLS functional is defined by

$$(2.6) \quad \tilde{\mathcal{G}}(\boldsymbol{\tau}, v; \mathbf{f}) = \|\operatorname{div} \boldsymbol{\tau} + Xv - f\|_{0,\Omega}^2 + \|A^{-1/2} \boldsymbol{\tau} + A^{1/2} \nabla v\|_{0,\Omega}^2.$$

It has been proved in [3] that the homogeneous FOSLS functional  $\tilde{\mathcal{G}}(\boldsymbol{\tau}, v; \mathbf{0})$  is coercive and bounded in  $\mathcal{V}_0$ , i.e., there exist positive constants  $c_1$  and  $c_2$  such that

$$(2.7) \quad c_1 \|\|(\boldsymbol{\tau}, v)\|\|^2 \leq \tilde{\mathcal{G}}(\boldsymbol{\tau}, v; \mathbf{0}) \leq c_2 \|\|(\boldsymbol{\tau}, v)\|\|^2$$

for all  $(\boldsymbol{\tau}, v) \in \mathcal{V}_0$ , where the FOSLS energy norm is given by

$$\|\|(\boldsymbol{\tau}, v)\|\| = (\|\boldsymbol{\tau}\|_{0,\Omega}^2 + \|\operatorname{div} \boldsymbol{\tau}\|_{0,\Omega}^2 + \|v\|_{1,\Omega}^2)^{1/2}.$$

The coercivity and boundedness of the homogeneous FOSLS functional further implies that the FOSLS minimization problem in (2.5) is well-posed, i.e., (2.5) has a unique solution.

**2.2. Treatment of Boundary Conditions.** Unlike finite element functions, it is not easy for a deep neural network function to satisfy a prescribed boundary condition. Such a difficulty was observed in [6] for the deep Ritz method. To circumvent this obstacle, for a Poisson equation (i.e.,  $A = I$  and  $X = 0$ ) with pure Dirichlet boundary conditions (i.e.,  $\Gamma_N = \emptyset$ ), they add the essential boundary conditions to the energy functional:

$$(2.8) \quad \tilde{\mathcal{J}}(v) = \int_{\Omega} \left( \frac{1}{2} |\nabla v(x)|^2 - f(x)v(x) \right) dx + \beta \|v(x) - g_D\|_{0,\partial\Omega}^2,$$

where  $\beta$  is a parameter to be determined. When the data vanishes, i.e.,  $f = 0$  and  $g_D = 0$ , the modified energy functional becomes

$$\tilde{\mathcal{J}}(v) = \frac{1}{2} \|\nabla v\|_{0,\Omega}^2 + \beta \|v(x)\|_{0,\partial\Omega}^2.$$

By the Sobolev trace theorem, the interior and boundary norms in the above formula are not in the same scale. Specifically, the boundary norm is 1/2-order weaker than the interior norm. This consideration suggests the following modified energy functional

$$(2.9) \quad \mathcal{J}(v; \mathbf{f}) = \frac{1}{2} \|\nabla v\|_{0,\Omega}^2 - \left( \int_{\Omega} f(x)v(x) dx + \int_{\Gamma_N} g_N v dS \right) + \beta \|v(x) - g_D\|_{1/2,\Gamma_D}^2$$

for the Poisson equation with the mixed boundary conditions in (2.2), where  $\mathbf{f} = (f, g_D, g_N)$  and  $\beta = \mathcal{O}(1)$  is a constant. The minimization problem based on the above energy functional is to find  $u \in H^1(\Omega)$  such that

$$(2.10) \quad \mathcal{J}(u; \mathbf{f}) = \min_{v \in H^1(\Omega)} \mathcal{J}(v; \mathbf{f}).$$

For the FOSLS formulation defined in (2.5), both the Dirichlet and Neumann boundary conditions are essential boundary conditions and, hence, we need to add them to the FOSLS functional with proper scales:

$$(2.11) \quad \begin{aligned} \mathcal{G}(\boldsymbol{\tau}, v; \mathbf{f}) &= \|\operatorname{div} \boldsymbol{\tau} + Xv - f\|_{0,\Omega}^2 + \|A^{-1/2}\boldsymbol{\tau} + A^{1/2}\nabla v\|_{0,\Omega}^2 \\ &+ \alpha_D \|v - g_D\|_{1/2,\Gamma_D}^2 + \alpha_N \|\mathbf{n} \cdot \boldsymbol{\tau} - g_N\|_{-1/2,\Gamma_N}^2 \end{aligned}$$

for all  $(\boldsymbol{\tau}, v) \in \mathcal{V} \equiv H(\operatorname{div}; \Omega) \times H^1(\Omega)$ , where  $\alpha_D = \mathcal{O}(1)$  and  $\alpha_N = \mathcal{O}(1)$  are constants and may be chosen to be one. Now, the corresponding FOSLS formulation is to find  $(\boldsymbol{\sigma}, u) \in \mathcal{V}$  such that

$$(2.12) \quad \mathcal{G}(\boldsymbol{\sigma}, u; \mathbf{f}) = \min_{(\boldsymbol{\tau}, v) \in \mathcal{V}} \mathcal{G}(\boldsymbol{\tau}, v; \mathbf{f}).$$

It has been proved that the homogeneous FOSLS functional  $\mathcal{G}(\boldsymbol{\tau}, v; \mathbf{0})$  is coercive and bounded in  $\mathcal{V}$ . This in turn implies that the LS minimization problem in (2.12) is well-posed in the space  $\mathcal{V}$  without strongly enforced boundary conditions.

For the LS functional defined in (1.1), the norm on boundary conditions is weaker than that for the equation; moreover, the Dirichlet and the Neumann boundary conditions are not treated differently. A balanced LS functional for problem (2.1) is as follows:

$$(2.13) \quad \mathcal{L}(v; \mathbf{f}) = \| -\operatorname{div}(A\nabla v) + Xv - f \|_{0,\Omega}^2 + \alpha_D \|v - g_D\|_{3/2,\Gamma_D}^2 + \alpha_N \|\mathbf{n} \cdot A\nabla v + g_N\|_{1/2,\Gamma_N}^2,$$

where  $\mathbf{f} = (f, g_D, g_N)$ . Now, the corresponding LS formulation is to find  $u \in H^2(\Omega)$  such that

$$(2.14) \quad \mathcal{L}(u; \mathbf{f}) = \min_{u \in H^2(\Omega)} \mathcal{L}(v; \mathbf{f}).$$

Assume that problem (2.1)-(2.2) is  $H^2$  regular. Then it is a direct consequence that the homogeneous LS functional  $\mathcal{L}(v; \mathbf{0})$  is coercive and bounded in  $H^2(\Omega)$ . This implies that problem (2.14) is well-posed.

*Remark 2.1.* Note that the LS formulation is only applicable to problems whose solutions are sufficiently smooth, more precisely, at least in  $H^2(\Omega)$ . This, in turn, implies that a DNN with non-piecewise-linear activation function is needed when using the LS functional as the loss function.

**3. The Deep FOSLS.** This section describes deep neural network structures and the deep FOSLS method. Discussions on numerical evaluation of the FOSLS functional are, in principle, valid for both the energy and the LS functionals. Moreover, similar error bound in (3.9) for the deep FOSLS is also valid for the energy and the LS functionals in the respective  $H^1$  and  $H^2$  norms.

**3.1. Deep Neural Network Structure.** A deep neural network is the compositions of multiple linear functions and activation functions. Specifically, the first component of DNN is a linear transformation  $T^l : \mathbb{R}^{n_l} \rightarrow \mathbb{R}^{n_{l+1}}$ :

$$(3.1) \quad T^l(x) = W^l x + b^l, \quad \text{for } x \in \mathbb{R}^{n_l},$$

where  $W^l = (w_{ij}^l) \in \mathbb{R}^{n_{l+1} \times n_l}$  and  $b^l \in \mathbb{R}^{n_{l+1}}$  are parameters to be determined. The second component is an activation function  $\psi : \mathbb{R} \rightarrow \mathbb{R}$  to be chosen. Application of  $\psi$  to a vector  $x \in \mathbb{R}^n$

is defined component-wisely, i.e.,  $\psi(x) = (\psi(x_i))$ . For an input  $x \in \mathbb{R}^d$ , a general  $(k + 1)$ -layer DNN, or a DNN with  $k$  hidden layers, from  $\mathbb{R}^d$  to  $\mathbb{R}^c$  can be represented as follows:

$$(3.2) \quad \mathcal{N}(x) = T^k \circ \psi \circ T^{k-1} \circ \psi \cdots \circ T^1 \circ \psi \circ T^0(x),$$

where  $d, c, k \in \mathbb{N}^+$  and  $n_0, \dots, n_{k+1} \in \mathbb{N}^+$  are positive integers with  $n_0 = d$  and  $n_{k+1} = c$ . The symbol  $\circ$  denotes the composition of functions:  $f \circ g(x) = f(g(x))$ . The total number of parameters of the DNN,  $\mathcal{N}(x)$ , defined in (3.2) is

$$(3.3) \quad N = \sum_{l=0}^k n_{l+1}(n_l + 1).$$

Activation function is a crucial component in deep learning. Choices of activation functions have influences on the output of a model, its accuracy, and the computational efficiency of training. A commonly used activation function is the Leaky ReLU defined as follows:

$$(3.4) \quad \psi(x) = \begin{cases} x, & \text{if } x > 0, \\ 0.01x, & \text{otherwise,} \end{cases}$$

which is a piecewise linear function. As discussed in [1, 13], a continuous piecewise linear function space with  $N$  dimensions is included in a deep neural network, with a piecewise linear function as the activation function, having at most  $\lceil \log_2(N + 1) \rceil$  hidden layers. By introducing some special network structures and adding more neurons as well as layers, a neural network is able to approximate a large class of functions other than linear [14]. Approximation theory on deep neural networks is still in its infancy.

In addition to piecewise linear activation functions such as ReLU, Leaky ReLU, etc., other types of activation functions have been used in practice. In this paper, we will also make use of the sigmoid function as an activation function, which is defined by

$$(3.5) \quad \psi(x) = \frac{1}{1 + e^{-x}}, \quad x \in \mathbb{R}.$$

Using a non-piecewise-linear activation function is essential for the deep LS method based on the LS functional defined in either (1.1) or (2.14). This is because functions generated by DNN with a piecewise linear activation function is only in  $H^1(\Omega)$ .

**3.2. Deep FOSLS.** The idea of the deep FOSLS is to employ a DNN for approximating the solution  $(\sigma(x), u(x))$  of the FOSLS minimization problem in (2.5). More specifically, for each  $x \in R^d$ , a DNN is implemented to compute an approximation  $(\hat{\sigma}(x, \Theta), \hat{u}(x, \Theta))$ , where  $\Theta \in R^N$  stands for all parameters in the DNN. A deep FOSLS approximation is to find  $(\hat{\sigma}(x, \Theta), \hat{u}(x, \Theta))$  such that

$$(3.6) \quad \mathcal{G}(\hat{\sigma}(x, \Theta), \hat{u}(x, \Theta); \mathbf{f}) = \min_{\Theta \in R^m} \mathcal{G}(\hat{\tau}(x, \Theta), \hat{v}(x, \Theta); \mathbf{f}).$$

Instead of evaluating the FOSLS functional analytically, in this paper we consider numerical approximation to the FOSLS functional. To this end, let  $\mathcal{T} = \{K : K \text{ is an open subset of } \Omega\}$  be a partition of the domain  $\Omega$ , i.e.,

$$\bar{\Omega} = \cup_{K \in \mathcal{T}} \bar{K} \quad \text{and} \quad K \cap T = \emptyset, \quad \forall K, T \in \mathcal{T}.$$

Let  $\mathcal{E}_D = \{E : E \text{ is an open subset of } \Gamma_D\}$  and  $\mathcal{E}_N = \{K : E \text{ is an open subset of } \Gamma_N\}$  be the partitions of  $\Gamma_D$  and  $\Gamma_N$ , respectively. Let  $x_K$  and  $x_E$  be interior points of  $K \in \mathcal{T}$  and  $E \in \mathcal{E}_S$  with  $S = D$  or  $N$ , respectively. Note that Sobolev norms  $\|\cdot\|_{1/2}$  and  $\|\cdot\|_{-1/2}$  in the FOSLS

functional are not computationally feasible and, hence, are approximated by weighted  $L^2$  norms with local weights  $h_E^{-1/2}$  and  $h_E^{1/2}$ , respectively, where  $h_E$  is the diameter of  $E$ . This idea leads to the following discrete FOSLS functional:

$$(3.7) \quad \hat{\mathcal{G}}(\hat{\boldsymbol{\tau}}(x, \Theta), \hat{v}(x, \Theta); \mathbf{f}) = \sum_{K \in \mathcal{T}} \left( (\operatorname{div} \hat{\boldsymbol{\tau}} + X \hat{v} - f)^2(x_K, \Theta) + (A^{-1/2} \hat{\boldsymbol{\tau}} + A^{1/2} \nabla \hat{v})^2(x_K, \Theta) \right) |K| \\ + \alpha_D \sum_{E \in \mathcal{E}_D} (\hat{v} - g_D)^2(x_E, \Theta) |E| h_E^{-1} + \alpha_N \sum_{E \in \mathcal{E}_N} (\mathbf{n} \cdot \hat{\boldsymbol{\tau}} - g_N)^2(x_E, \Theta) |E|^3 h_E,$$

where  $|K|$  and  $|E|$  are the  $d$  and  $d - 1$  dimensional measures of  $K$  and  $E$  respectively; and  $\alpha_D$  and  $\alpha_N$  are two positive parameters. Then the discrete deep FOSLS approximation is to find  $(\hat{\boldsymbol{\sigma}}(x, \Theta), \hat{u}(x, \Theta))$  such that

$$(3.8) \quad \hat{\mathcal{G}}(\hat{\boldsymbol{\sigma}}_\tau(x, \Theta), \hat{u}_\tau(x, \Theta); \mathbf{f}) = \min_{\Theta \in R^m} \hat{\mathcal{G}}(\hat{\boldsymbol{\tau}}(x, \Theta), \hat{v}(x, \Theta); \mathbf{f}).$$

To understand approximation property of the discrete deep FOSLS, by the triangle inequality, we have

$$(3.9) \quad \|\|(\boldsymbol{\sigma} - \hat{\boldsymbol{\sigma}}_\tau, u - \hat{u}_\tau)\|\| \leq \|\|(\boldsymbol{\sigma} - \hat{\boldsymbol{\sigma}}, u - \hat{u})\|\| + \|\|(\hat{\boldsymbol{\sigma}} - \hat{\boldsymbol{\sigma}}_\tau, \hat{u} - \hat{u}_\tau)\|\|,$$

where the first term represents the approximation error caused by the deep neural network and the second term is the numerical error by evaluating the FOSLS functional. How to estimate the former is still an open problem. The latter can be computed to a desired accuracy through either uniform or adaptive partition of the  $\Omega$ ,  $\Gamma_D$ , and  $\Gamma_N$ . A detailed algorithmic and theoretical discussions of the second term will be presented in a forthcoming paper.

**4. Numerical Experiments.** The solution  $u(x)$  and the flux  $\boldsymbol{\sigma}(x)$  in the FOSLS formulation are independent variables. This observation implies that an efficient training strategy is to treat them as two separate training targets. Hence, the deep neural network to be employed consists of two branches: the upper and lower branches for the respective  $u$  and  $\boldsymbol{\sigma}$  (see Figure 4.1). These two branches have no neuron connection. For numerical experiments in this paper, we use a four layer neural network. Within each branch, a fully connected layer is implemented. All parameters of the neural network are trained simultaneously with the single discrete FOSLS functional as the loss function. In the training process, Adam optimizer version of gradient descent [8] is implemented.

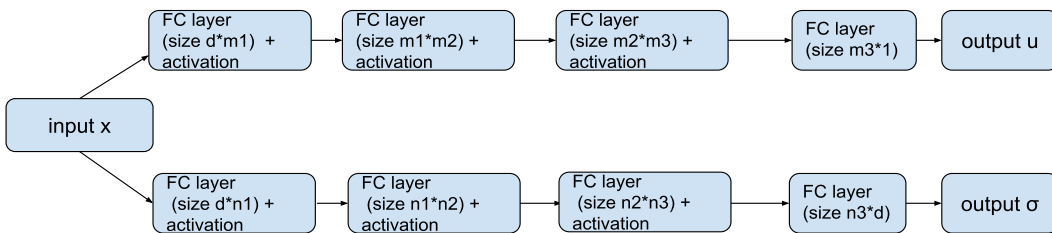


FIG. 4.1. Four-layer neural network for training  $u(x)$  and  $\boldsymbol{\sigma}(x)$

Let  $\Theta_u$  and  $\Theta_\sigma$  represent all parameters in the upper and lower branches, respectively. Denote by  $T_u^l$  and  $T_\sigma^l$  the linear transformation defined in (3.1) for the respective upper and lower branches and by  $\psi$  the activation function defined in (3.4) or (3.5). Then the composition of the activation function and the linear transformation for the  $l$ -th block in the respective upper and lower branches are

$$(4.1) \quad \mathcal{N}_u^l = \psi(T_u^l(x)) \quad \text{and} \quad \mathcal{N}_\sigma^l = \psi(T_\sigma^l(x)).$$

Then the deep FOSLS method defines mappings from  $x$  to  $u(x, \Theta_u)$  by the upper branch and to  $\sigma(x, \Theta_\sigma)$  by the lower branch:

$$u(x, \Theta_u) = T_u^4(\mathcal{N}_u^3 \circ \mathcal{N}_u^2 \circ \mathcal{N}_u^1(x)) \quad \text{and} \quad \sigma(x, \Theta_\sigma) = T_\sigma^4(\mathcal{N}_\sigma^3 \circ \mathcal{N}_\sigma^2 \circ \mathcal{N}_\sigma^1(x)).$$

Both the deep LS and Ritz methods define mappings from  $x$  to  $u(x, \Theta_u)$  by the upper branch.

Test problems in this section consist of the Poisson and singularly perturbed reaction-diffusion equations and an interface problem in one dimension. The Leaky ReLU and Sigmoid are used for both the deep Ritz and FOSLS methods, while the deep LS method may only use the Sigmoid.

Numerical results are reported through the true error in the relative  $L^2$  norm and the  $H^1$  seminorm (see Tables 4.2, 4.3 and 4.4). Moreover, the exact solution vs numerical approximations are depicted in Figures 4.2, 4.3 and 4.4. Note that only the figures for the FOSLS functional are presented as reference in Figures 4.2 and 4.3 since results for the Energy and the LS functionals are similar. For the deep FOSLS method, we also report numerical results on the approximation to the flux variable in the relative  $L^2$  norm and on the relative FOSLS functional. As discussed in section 3.2, the FOSLS functional, similarly the energy and the LS functionals, are evaluated numerically based on a partition of the domain. For one-dimensional examples in this section, we use an uniform partition of interval  $[a, b]$ .

**4.1. Poisson Equation.** The first test problem is the Poisson equation:

$$(4.2) \quad \begin{cases} -u''(x) = f(x), & x \in \Omega = (0, 1), \\ u = 0, & x \in \partial\Omega = \{0, 1\}. \end{cases}$$

For  $f = -40000(x^3 - 2x^2/3 + 173x/1800 + 1/300)e^{-100(x-1/3)^2}$ , problem (4.2) has the following exact solution

$$u(x) = x \left( e^{-(x-\frac{1}{3})^2/0.01} - e^{-\frac{4}{9}/0.01} \right).$$

This is a test problem used in [7].

A four-layer neural network depicted in Figure 4.1 is implemented for the deep FOSLS method. Each block in the first layer is constructed with 24 neurons, and each block in the middle two layers has 14 neurons. The output layers of  $u$  and  $\sigma$  have 1 and  $d$  neurons, respectively, where  $d$  is the dimension of the underlying problem. For  $d = 1$ , the total number of parameters of this two-branch network is 1246. Activation functions are selected as the Leaky ReLU and Sigmoid. For approach based on the energy and LS functionals, only the upper branch of the network is used.

To numerically evaluate the functionals, the interval  $[0, 1]$  is partitioned into a set of equal-length subintervals. Denote  $h$  as the size of each subinterval, then the integrals and first-order derivatives in the functionals are approximated by the midpoint rule and the forward finite difference quotient,  $\frac{u(x+dx) - u(x)}{dx}$ , with  $dx = h/2$ , respectively. The coefficient  $\beta$  of the boundary integrals in the functionals is  $1/h$  accordingly. A fixed learning rate 0.0005 is used for the gradient decent minimization algorithm. All experiments are replicated three times to reduce variability. After training 10000 epochs for each phase, the medians of three training results are reported in Table 4.2 and Figure 4.2.

With a fixed DNN structure described above, the goal of the first numerical experiment is to show that with sufficiently fine mesh for evaluating the FOSLS functional, accuracy of the deep FOSLS method is determined by the approximation property of the DNN structure. Using the Leaky ReLU and 10000 as the training epochs, Table 4.1 shows that 800 sampling points are enough to accurately evaluate the FOSLS functional.

Table 4.2 shows that all three methods are able to accurately approximate the solution of the Poisson equation. Moreover, DNN using the Sigmoid is more accurate and efficient than that using the Leaky ReLU.



TABLE 4.1  
Relative errors of Poisson equation with different number of sampling points

Relative errors Sampling points	$\frac{\ u - u_k\ _0}{\ u\ _0}$	$\frac{ u - u_k _1}{ u _1}$	$\frac{\ \sigma - \sigma_k\ _0}{\ \sigma\ _0}$	$\frac{G(\sigma_k, u_k; \mathbf{f})}{\ (\sigma, u)\ ^2}$
200	0.065238	0.109056	0.056508	0.00961
400	0.048421	0.167703	0.026564	0.00912
800	0.025238	0.106552	0.020481	0.00472
1600	0.024631	0.114932	0.020091	0.00402

TABLE 4.2  
Relative errors of Poisson equation with different functionals, activation functions and sampling points

Relative errors Loss and activation	$\frac{\ u - u_k\ _0}{\ u\ _0}$	$\frac{ u - u_k _1}{ u _1}$	$\frac{\ \sigma - \sigma_k\ _0}{\ \sigma\ _0}$	$\frac{G(\sigma_k, u_k; \mathbf{f})}{\ (\sigma, u)\ ^2}$
Energy (LeakyReLU & 800 points)	0.029161	0.160666	—	—
FOSLS (LeakyReLU & 800 points)	0.025238	0.106552	0.020481	0.00472
Energy (Sigmoid & 200 points)	0.013144	0.026246	—	—
LS (Sigmoid & 200 points)	0.008876	0.009108	—	—
FOSLS (Sigmoid & 200 points)	0.013505	0.019830	0.008897	0.002084

**4.2. Singularly Perturbed Reaction-Diffusion Equation.** The second test problem is the singularly perturbed reaction-diffusion equation:

$$(4.3) \quad \begin{cases} -\varepsilon^2 u''(x) + u(x) = f(x), & x \in \Omega = (-1, 1), \\ u = 0, & x \in \partial\Omega = \{-1, 1\}. \end{cases}$$

For  $f = -2(\varepsilon - 4x^2 \tanh(\frac{1}{\varepsilon}(x^2 - \frac{1}{4}))) (1/\cosh(\frac{1}{\varepsilon}(x^2 - \frac{1}{4})))^2 + \tanh(\frac{1}{\varepsilon}(x^2 - \frac{1}{4})) - \tanh(\frac{3}{4\varepsilon})$ , problem (4.3) has the following exact solution

$$u(x) = \tanh\left(\frac{1}{\varepsilon}(x^2 - \frac{1}{4})\right) - \tanh\left(\frac{3}{4\varepsilon}\right).$$

With  $\sigma = -\varepsilon^2 u'$ , the corresponding FOSLS functional defined in (2.3) is of the form

$$\mathcal{G}(\tau, v; f) = \|\tau' + v - f\|_0^2 + \|(\tau/\varepsilon + \varepsilon v')\|_0^2 + \alpha \|u\|_{1/2, \partial\Omega}^2.$$

Similarly, a four-layer neural network depicted in Figure 4.1 is implemented. Each block in the first and middle two layers has 32 and 24 neurons, respectively. The output layers of  $u$  and  $\sigma$  both have 1 neuron in one dimension. This network has 2962 parameters. Numerical evaluations of the functionals are done on a uniform partition of the interval  $[-1, 1]$  with mesh size  $h = 0.001$ . An adaptive learning rate is used for the gradient decent process. Starting with 0.001, learning rate is reduced by half for every 5000 epochs.

For  $\varepsilon = 0.01$ , with 20000 training epochs for each phase and all experiments being repeated three times, the medians of three results are reported in Table 4.3 and Figure 4.3. All three methods exhibit accurate approximation to the solution with interior layers. For both the Leaky ReLU and Sigmoid, the deep FOSLS method is about twice more accurate than the deep Ritz method. Again, the DNN using the Sigmoid is more accurate than that using the Leaky ReLU.

**4.3. Interface Problem.** The third test problem is an interface problem as follows.

$$(4.4) \quad \begin{cases} -(\alpha u'(x))' = f(x), & x \in \Omega = (0, 1), \\ u = 0, & x \in \partial\Omega = \{0, 1\}, \end{cases}$$



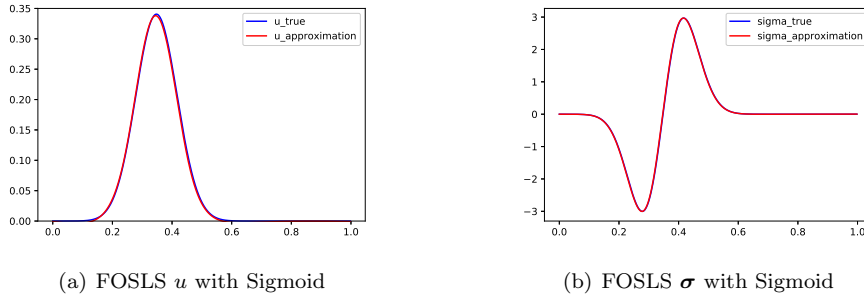


FIG. 4.2. Poisson equation approximation results with FOSLS functional and sigmoid activation

TABLE 4.3  
Relative errors of singular perturbed equation with different loss and activation functions

Relative errors Loss and activation	$\frac{\ u - u_k\ _0}{\ u\ _0}$	$\frac{ u - u_k _1}{ u _1}$	$\frac{\ \sigma - \sigma_k\ _0}{\ \sigma\ _0}$	$\frac{G(\sigma_k, u_k; \mathbf{f})}{\ (\sigma, u)\ ^2}$
Energy functional (LeakyReLU)	0.011316	0.026179	—	—
FOSLS functional (LeakyReLU)	0.006654	0.020810	0.099863	0.0047
Energy functional (Sigmoid)	0.003019	0.004612	—	—
LS functional (Sigmoid)	0.000910	0.002088	—	—
FOSLS functional (Sigmoid)	0.001403	0.001711	0.211490	0.003766

where  $\alpha = 1$  for  $x \in (0, \frac{1}{2})$  and  $\alpha = k$  for  $x \in (\frac{1}{2}, 1)$ . It is well-known that solutions of interface problems are not smooth, in particular, not in  $H^2(\Omega)$ . For

$$f(x) = \begin{cases} 8k(3x - 1), & x \in (0, \frac{1}{2}), \\ 4k(k + 1), & x \in (\frac{1}{2}, 1), \end{cases}$$

problem (4.4) has the following exact solution

$$u(x) = \begin{cases} 4kx^2(1 - x), & x \in (0, \frac{1}{2}), \\ [2(k + 1)x - 1](1 - x), & x \in (\frac{1}{2}, 1). \end{cases}$$

With  $\sigma = -\alpha u'$ , the corresponding FOSLS functional defined in (2.3) has the form of

$$\mathcal{G}(\tau, v; f) = \|\tau' - f\|_0^2 + \|(\alpha^{-\frac{1}{2}}\tau + \alpha^{\frac{1}{2}}v')\|_0^2 + \beta \|u\|_{1/2, \partial\Omega}^2.$$

The same network structure with the Sigmoid is implemented for the interface problem as the one used for the singularly perturbed equation. Numerical evaluations of the functionals are done on a uniform partition of the interval  $[0, 1]$  with mesh size  $h = 0.002$ . An adaptive learning rate is used for the gradient decent process. Starting with 0.01, learning rate is reduced by half for every 5000 epochs.

For  $k = 10$ , with 20000 training epochs for each phase and all experiments being replicated three times, the medians are reported in Table 4.4 and Figure 4.4. The results show that the deep FOSLS method is significant better than the deep Ritz method and that the deep LS method fails to approximate the solution well. This verifies Remark 2.1, i.e., the deep LS method is only applicable to sufficiently smooth problems.

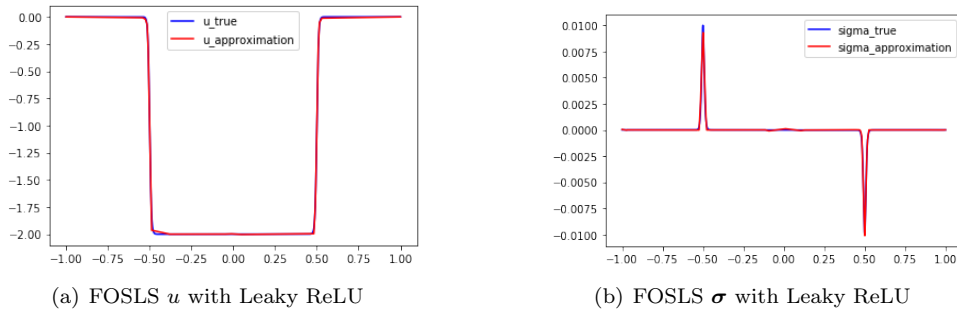
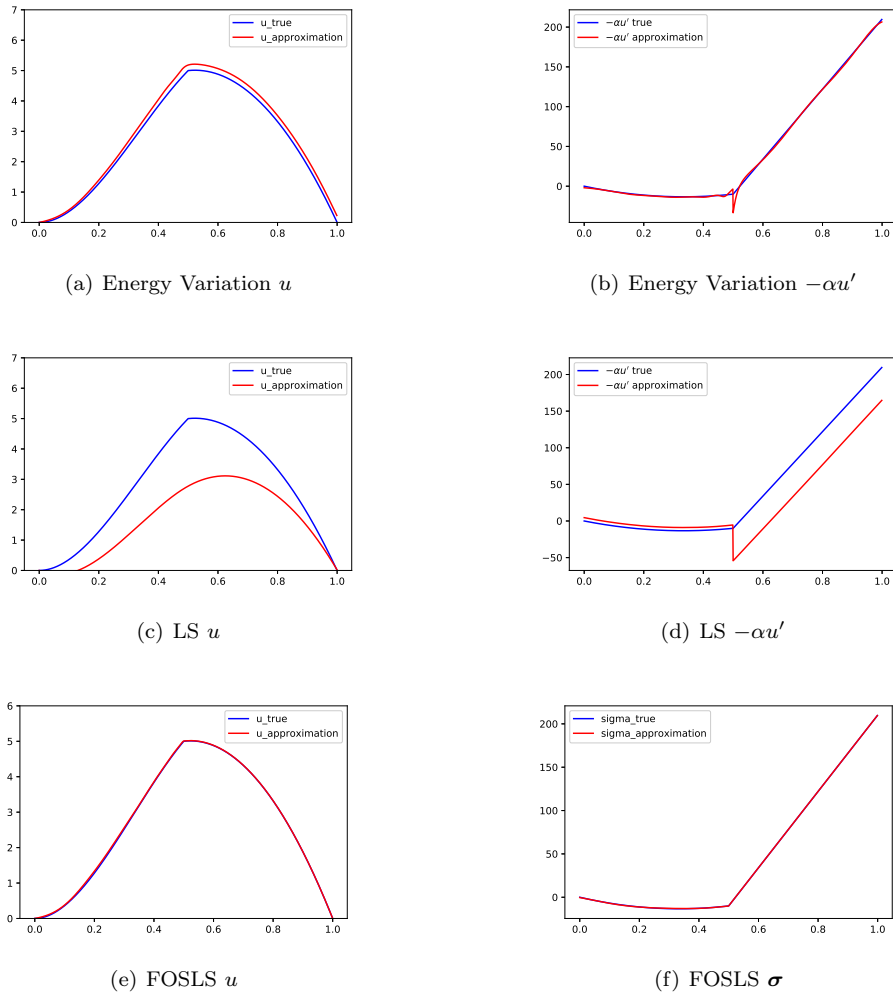
FIG. 4.3. *Singular perturbed equation approximation results with FOSLS functional and Leaky ReLU*FIG. 4.4. *Interface problem approximation results with different loss functions*

TABLE 4.4  
Relative errors of interface problem with different loss functions

Loss function	Relative errors			
	$\frac{\ u - u_k\ _0}{\ u\ _0}$	$\frac{ u - u_k _1}{ u _1}$	$\frac{\ \sigma - \sigma_k\ _0}{\ \sigma\ _0}$	$\frac{G(\sigma_k, u_k; \mathbf{f})}{\ (\sigma, u)\ ^2}$
Energy functional (Sigmoid)	0.054705	0.068104	—	—
LS functional (Sigmoid)	0.397965	0.397506	—	—
FOSLS functional (Sigmoid)	0.007137	0.004565	0.001870	0.005073

**5. Discussion and Conclusion.** We proposed the deep FOSLS method by using DNNs to approximate solutions of PDEs and modified the deep Ritz and the deep LS methods by treating boundary conditions in a balance way. While the deep Ritz and LS methods are only applicable to problems having underlying minimization principle and smooth problems, respectively, the deep FOSLS method is applicable to a much larger class of problems.

Both the deep LS and FOSLS methods are based on the least-squares principle applied to the respective original PDEs and a first-order system of the original PDEs. A striking feature of the least-squares principle is that values of the LS and FOSLS functionals provide feedback for automatically controlling numerical processes such as the numbers of neurons and layers in DNN, the number and the location of sampling points for evaluating the functionals. Adaptive control first on numerical evaluation of the least-squares functionals and then on DNN structure will be topics of our study on the deep least-squares methods. Finally, unlike finite elements, DNN generates function in  $H^2(\Omega)$  when using non-piecewise-linear activation function. This means that the deep LS method is a competitive method for smooth problems.

With limited knowledge on approximation theory of DNNs, in order to accurately evaluate the functionals, inequality (3.9) and similar inequalities in the  $H^1$  and  $H^2$  norms for the respective deep Ritz and LS methods shed some lights on how to choose sampling points for a fixed DNN structure.

#### REFERENCES

- [1] R. Arora, A. Basu, P. Mianjy, and A. Mukherjee. Understanding deep neural networks with rectified linear units. *arXiv preprint arXiv:1611.01491*, 2016.
- [2] J. Berg and K. Nystrom. A unified deep artificial neural network approach to partial differential equations in complex geometries. *Neurocomputing*, 317:28–41, 2018.
- [3] Z. Cai, R. Lazarov, T. A. Manteuffel, and S. F. McCormick. First-order system least squares for second-order partial differential equations: Part i. *SIAM Journal on Numerical Analysis*, 31(6):1785–1799, 1994.
- [4] M. W. M. G. Dissanayake and N. Phan-Thien. Neural network based approximations for solving partial differential equations. *Communications in Numerical Methods in Engineering*, 10(3):195–201, 1994.
- [5] T. Dockhorn. A discussion on solving partial differential equations using neural networks. *CoRR*, abs/1904.07200, 2019.
- [6] W. E and B. Yu. The deep ritz method: A deep learning-based numerical algorithm for solving variational problems. *Communications in Mathematics and Statistics*, 6(1), 3 2018.
- [7] J. He, L. Li, J. Xu, and C. Zheng. Relu deep neural networks and linear finite elements. *arXiv preprint arXiv:1807.03973*, 2018.
- [8] D. P. Kingma and J. Ba. Adam: A method for stochastic optimization. *arXiv preprint arXiv:1412.6980*, 2014.
- [9] I. E. Lagaris, A. Likas, and D. I. Fotiadis. Artificial neural networks for solving ordinary and partial differential equations. *IEEE Transactions on Neural Networks*, 9(5):987–1000, 1998.
- [10] I. E. Lagaris, A. C. Likas, and D. G. Papageorgiou. Neural-network methods for boundary value problems with irregular boundaries. *IEEE Transactions on Neural Networks*, 11(5):1041–1049, 2000.
- [11] K. S. McFall and J. R. Mahan. Artificial neural network method for solution of boundary value problems with exact satisfaction of arbitrary boundary conditions. *IEEE Transactions on Neural Networks*, 20(8):1221–1233, 2009.
- [12] J. Sirignano and K. Spiliopoulos. Dgm: A deep learning algorithm for solving partial differential equations. *Journal of Computational Physics*, 375:1139–1364, 2018.

- [13] J. Tarela and M. Martinez. Region configurations for realizability of lattice piecewise-linear models. *Mathematical and Computer Modelling*, 30(11-12):17–27, 1999.
- [14] D. Yarotsky. Error bounds for approximations with deep relu networks. *Neural Networks*, 94:103–114, 2017.